

ABOUT MODELLING OF EMPIRICAL CORRELATIONS WITHIN AERODYNAMIC PROFILES USING HIGHER ORDER ARTIFICIAL NEURAL NETWORKS

Patrik Kovář^{1, 2} & Jiří Fürst¹

Department of Technical Mathematics, Faculty of Mechanical Engineering, Czech Technical University in Prague, Karlovo náměstí 13, Praha 2, 120 00, Czech republic, Mailbox: Patrik.Kovar@fs.cvut.cz
 Center of Aviation and Space Research, Faculty of Mechanical Engineering, Czech Technical University in Prague, Jugoslávských partyzánů 1580/30, Praha 6, 160 00, Czech republic

Abstract

Nowadays, numerical simulations remain time-consuming. Consequently, empirical correlations keep their importance as a valuable tool for compressor design and for estimating flow parameters. This contribution utilizes higher order neural networks to predict flow parameters for new family of airfoils, offering an alternative to time-expensive simulations or inaccurate empirical correlations.

Keywords: compressor cascade, empirical correlations, optimization, machine learning, neural networks

1. Motivation

Axial compressor is a key component of every state of the art turboprop engine. It delivers compressed air into the combustion chamber to maximize effectiveness of the fuel combustion, that enables lower amount of the fuel necessary to the flight mission. Nowadays, as demand for advanced technologies in aircraft industry is increasing, a need for profiles in the axial compressor that perform better than classical profiles is also increasing.

Classical profiles as NACA 65-series and C.4 circular-arc are appropriate for low Mach numbers, corresponding to subsonic flows. Double-circular arc (DCA) and multi-circular arc (MCA) profiles exhibit good performance when the flow is accelerated to high subsonic or even low supersonic velocities [1]. Specifically designed for subsonic and transonic cascade applications, Controlled Diffusion (CD) airfoils can offer superior performance compared to DCA or MCA profiles. The CD airfoils are constructed to shape the blade beyond the peak suction point of the surface velocity, minimizing loss for the airfoil section [2]. The new family of airfoils introduced in [3] is expected to outperform the classical NACA 65-series, show comparable performance to CD airfoils, and offer a significantly wider range of acceptable incidence angles before stalling occurs. The design of the camber line and thickness distribution of the profile is based on the desired pressure distribution on the blade surface.

Despite computational fluid dynamics (CFD) being time-consuming, empirical correlations remain a common tool for designing and predicting axial compressor cascade performance. Unfortunately, there is insufficient experimental data for families of airfoils other than the classical profiles, leading to a lack of correlations for these profiles. This contribution focuses on the modelling of correlations for flow parameters estimation within compressor cascade and its ability to optimize geometry of the axial compressor blades at the design operational point.

Present contribution deals with a novel approach for the investigation of flow field within axial compressor, that is based on the solution of radial equilibrium equation and empirical correlations. A set of very comprehensive and precise CFD simulations were performed in order to replace expensive measurements. Proposed method, in context of practical applications, is also discussed and it turned out as promising approach to further work.

2. Objective statement

Initially, let's introduce the geometric parameters within the compressor cascade. As depicted on the left-hand side of Figure 1, the parameter c corresponds to the blade chord, while parameters a and b indicate the point where the maximum of the camber line is reached. Symbols χ_1 and χ_2 represent blade angles in relation to the chord line. Subscripts "1" and "2" are utilized to differentiate between conditions at the blade's inlet and discharge, respectively. The angle θ is the sum of blade angles, expressed as $\theta = \chi_1 + \chi_2$.

In the context of the cascade (Figure 1 right), there exists a stagger or setting angle γ , which represents the angle between the chord line and the axial direction, and blade angles κ_1 , κ_2 , indicating the angles between the camber line and the axial direction at the leading and trailing edges respectively. The blade density is defined by the solidity $\sigma = c/s$. The flow is characterized by velocities W_1 , W_2 , and flow angles β_1 , β_2 with respect to the axial direction. Additionally, parameters such as the incidence angle i, deviation angle δ , and angle of attack α are defined in [1]

$$\alpha = \beta_1 - \gamma, \quad i = \beta_1 - \kappa_1, \quad \delta = \beta_2 - \kappa_2, \kappa_1 = \chi_1 + \gamma, \quad \kappa_2 = \gamma - \chi_2. \tag{1}$$

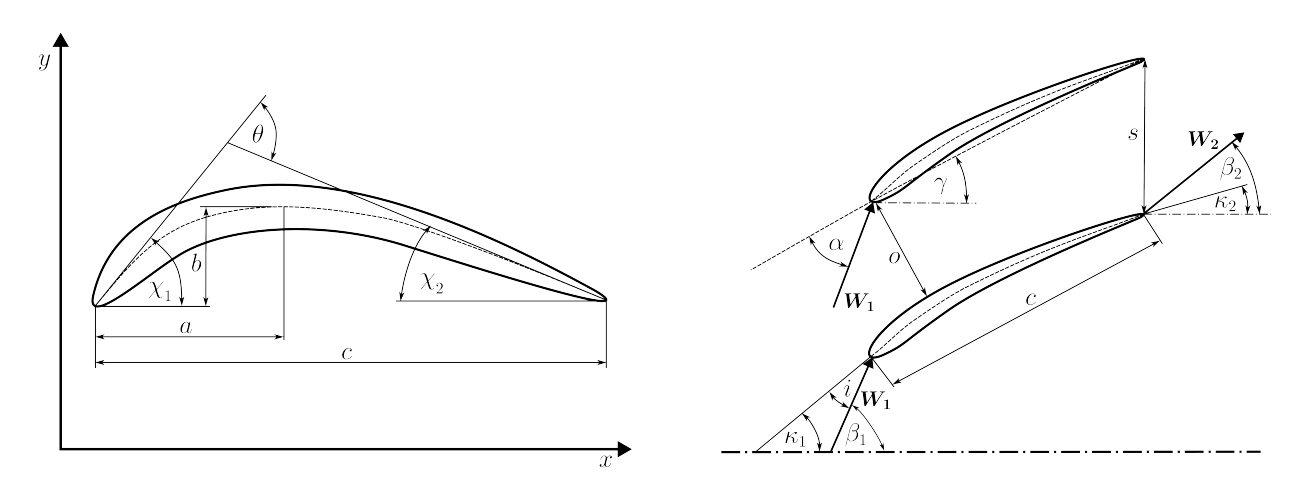


Figure 1 – Cascade nomenclature: profile parameters (left); cascade and flow parameters (right).

2.1 An approach by employing CFD

Computational fluid dynamics (CFD) has become a valuable method for flow analysis, design, and optimization in recent years. Despite advancements in computational power, performing a series of numerical simulations can still be quite demanding. To determine conditions at the design point, it is essential to identify the correct value for the design incidence angle i^* , as illustrated in Figure 2. In Figure 2 (right), the procedure for finding a design point is outlined. The process involves conducting simulations with various boundary conditions and loss evaluations, aiming to identify the point with the minimum pressure loss (PL), that is impractical due to the computational complexity mentioned earlier.

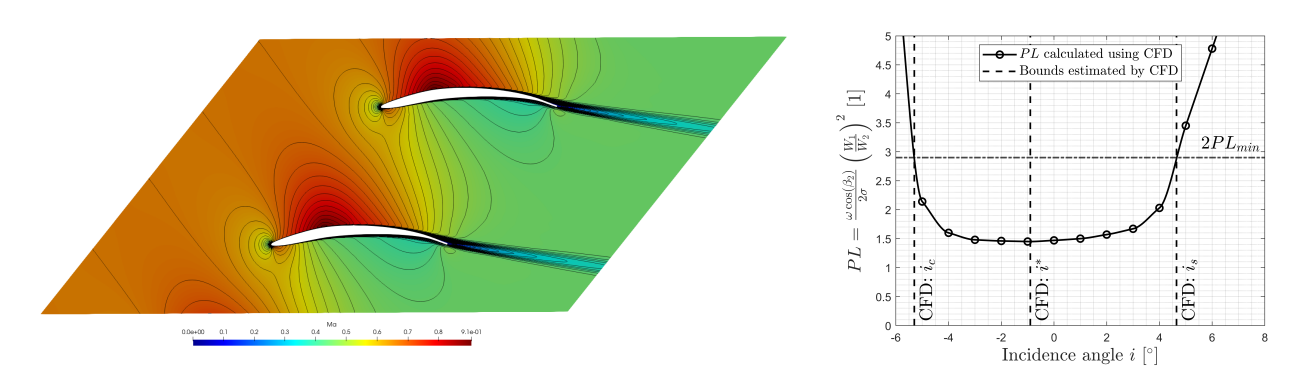


Figure 2 – CFD post processing: flow field example (left); design point finding (right).

2.2 Computational method

Computational method is based on Euler equations for axisymmetric flow. The calculation is performed in meridional plane in curvilinear coordinate system $\{m,y\}$. Quasi-normals correspond to an inlet cross-section and leading and trailing edges of blade rows as it is shown in Figure 3. Shapes of the stream surfaces are determined during the calculation.

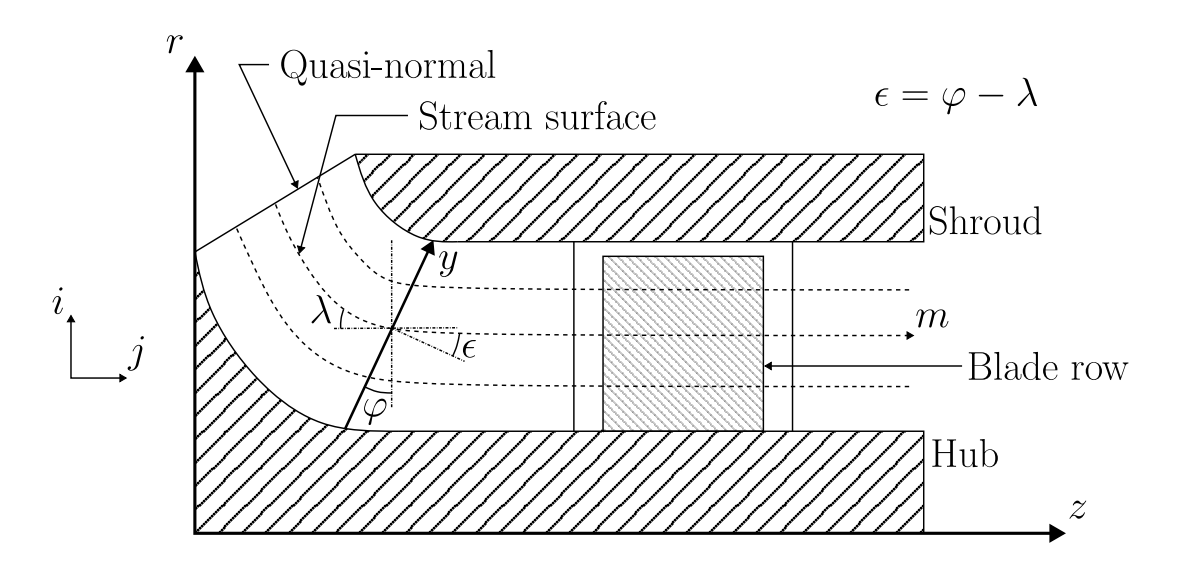


Figure 3 – Curvilinear coordinate system.

2.2.1 Calculation on inlet cross-section

Based on prescribed boundary conditions for total pressure $p_{t,in}$, total temperature $T_{t,in}$ and mass flow $m_{t,in}$, entropy s_{in} and total enthalpy $H_{t,in}$ are determined using p-T diagrams. Meridional component of the velocity is obtained by solving non-linear equation in order to reach desired mass flow as

$$\dot{m}_{in} = \int_0^{y_s} 2\pi r \rho_{in} C_{m,in} \cos \varepsilon dy, \tag{2}$$

where density at the inlet ρ_{in} is determined using h-s diagram. Tangential component of the velocity is equal to zero and the rest of quantities are determined using thermodynamic relations.

2.2.2 Calculation on the quasi-normal cross-sections without blades

In case of quasi-normal without blades, tangential component of the velocity is determined using moment of momentum conservation. Furthermore, entropy s and total enthalpy H_t remains constant along the streamline. The rest of quantities are obtained through solution of radial equilibrium

$$\frac{\partial W_m}{\partial y} = f_1(y)W_m + f_2(y) + \frac{f_3(y)}{W_m},\tag{3}$$

where functions $f_{\{1,2,3\}}$ are defined, according to [1], as

$$f_1(y) = -\kappa_m \cos \varepsilon + \frac{\sin \varepsilon}{W_m} \frac{\partial W_m}{\partial m},$$

$$f_2(y) = 0,$$

$$f_3(y) = \frac{\partial H}{\partial y} - T \frac{\partial s}{\partial y} \frac{C_{\varphi}}{r} \frac{\partial (rC_{\varphi})}{\partial y}.$$
(4)

An approximation of the meridional gradient of C_m can be computed as

$$\frac{1}{W_m} \frac{\partial W_m}{\partial m} \left(1 - M_m^2 \right) = -\left(1 + M_{\varphi}^2 \right) \frac{\sin \varphi}{r} - \frac{1}{\cos \varepsilon} \frac{\partial \varphi}{\partial y} - \kappa_m \tan \varepsilon, \tag{5}$$

where $\kappa_m = -\partial \varphi/\partial m$ is a streamline curvature, $M_m = C_m/a$, $M_{\varphi} = C_{\varphi}/a$ are meridional and tangential Mach numbers, respectively, and symbol a denotes speed of sound.

2.2.3 Calculation on the quasi-normal cross-sections with blades

The calculation is performed in relative coordinate system in case of quasi-normal that corresponds to blade cross-section. When stator blade row is computed, rotational speed $\omega=0$. Total rothalpy I_t is also conserved similarly as in the case without blades. Flow angles β can be determined using empirical correlations and values from the previous iteration. Pressure loss is also obtained using empirical correlation and then it is recalculated into entropy increasement Δs . The rest of quantities are also obtained through solution of radial equilibrium equation (3) with $f_{\{1,2,3\}}$

$$f_{1}(y) = \cos^{2}\beta' \left[-\kappa_{m}\cos\varepsilon - \frac{\tan\beta'}{r} \frac{\partial(r\tan\beta')}{\partial y} + \frac{\sin\varepsilon}{W_{m}} \frac{\partial W_{m}}{\partial m} \right]$$

$$f_{2}(y) = -2\omega\cos\beta'\sin\beta'\cos\lambda$$

$$f_{3}(y) = \cos^{2}\beta' \left[\frac{\partial I}{\partial y} - T \frac{\partial s}{\partial y} \right]$$
(6)

2.2.4 Streamline shape corrections

Shape of streamlines are corrected after the calculation on whole streamline sets is performed. New streamline positions y are computed in order to preserve equality

$$\int_0^{y(i,j)} 2\pi r \rho C_m \cos \varepsilon dy = \dot{m}_{in} \frac{j-1}{NS-1},\tag{7}$$

where NS refers to number of streamlines and j denoted individual streamline, i.e., $j = \{1, ..., NS\}$. When inlet boundary conditions are set, parameters at the inlet can be computed. Initial stream surfaces are equally spaced. Flow field parameters at individual quasi-normals are calculated using aforementioned procedure. After that, stream line positions are corrected if necessary. Then the process is repeated until the flow field is converged as it can be seen on workflow in Figure 4.

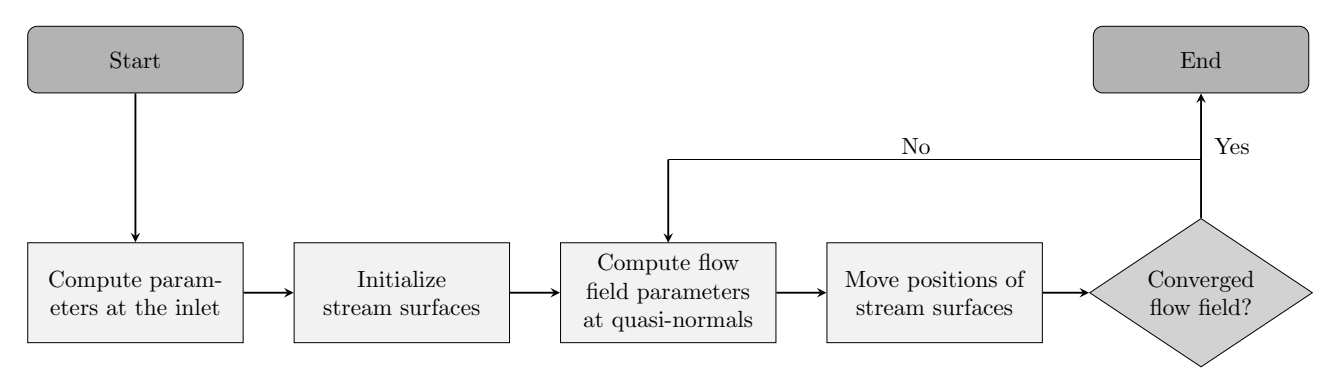


Figure 4 – Workflow of the procedure.

2.3 An approach by employing empirical correlations

In the past, the primary goal of the empirical modeling process was to forecast fluid turning and total pressure loss for a cascade under relatively broad operating conditions, as reported in [1]. Empirical correlations were developed based on experimental data derived from two-dimensional measurements conducted on classical profiles such as the NACA-65 series and C.4 profiles.

To emphasize level of non-linearity and complexity of the task, there are documented empirical correlation for important flow parameters in the compressor cascade as the design incidence angle i^* and resulting pressure loss PL after the flow throughout the cascade.

2.3.1 Design angle of attack α^* and incidence angle i^*

The design angle of attack α^* , or the design incidence angle i^* , define a near-optimum or minimum-loss inlet angle for the cascade. The selection of α^* was based on achieving smooth blade surface pressure distributions, particularly on the suction surface. Herrig has formulated the following empirical model in [4]

$$\alpha^* = \left(3.6K_{sh}K_{t,i} + 0.3532\theta \left(\frac{a}{c}\right)^{0.25}\right)\sigma^e, \quad e = 0.65 - 0.002\theta, \tag{8}$$

where correction factor K_{sh} is assumed as constant for specific family of airfoils and parameter $K_{t,i}$ can be correlated as a function of maximal blade thickness-to-chord ratio t_b/c [1]

$$K_{t,i} = \left(10\frac{t_b}{c}\right)^q, \quad q = 0.28/\left(0.1 + (t_b/c)^{0.3}\right).$$
 (9)

Design incidence angle *i** correlation was developed by Lieblein in [5]

$$i^* = K_{sh}K_{t,i}(i^*)_{(10)} + n\theta. {10}$$

The first term on the right-hand side is the design incidence angle for a camber angle of zero. It is computed from a correlation for NACA 65-series blades and corrected by K_{sh} and $K_{t,i}$

$$(i_0^*)_{(10)} = \frac{\beta_1^p}{5 + 46\exp(-2.3\sigma)} - 0.1\sigma^3 \exp\left(\frac{\beta_1 - 70}{4}\right), \quad p = 0.914 + \frac{\sigma^3}{160}.$$
 (11)

According to [6], the slope factor n can be expressed as

$$n = 0.025\sigma - 0.06 - \frac{(\beta_1/90)^{(1+1.2\sigma)}}{1.5 + 0.43\sigma}.$$
 (12)

2.4 Design deviation angle δ^*

There is also an empirical model for the design deviation angle δ^* supplied by Lieblein [7] that corresponds to operation at the design incidence angle i^* . The model has similar form as design incidence angle correlation discussed above

$$\delta^* = K_{sh}K_{t,\delta}(\delta_0^*)_{(10)} + m\theta. \tag{13}$$

Coefficient K_{sh} is the same as for the design incidence angle model and parameter $K_{t,\delta}$ is correlated as

$$K_{t,\delta} = 6.25 \left(\frac{t_b}{c}\right) + 37.5 \left(\frac{t_b}{c}\right)^2. \tag{14}$$

Design zero-camber deviation angle $(\delta_0^*)_{(10)}$ from Johnsen and Bullock [6] can be obtained as

$$(\delta_0^*)_{(10)} = 0.01\sigma\beta_1 + (0.74\sigma^{1.9} + 3\sigma) \left(\frac{\beta_1}{90}\right)^{(1.67 + 1.09\sigma)}.$$
 (15)

Defining $x = 0.01\beta_1$, the slope factor m for the NACA 65-series camberline is modelled as [1]

$$m = \frac{m_{1.0}}{\sigma^b}, \quad m_{1.0} = 0.17 - 0.0333x + 0.333x^2, \quad b = 0.9625 - 0.17x - 0.85x^3.$$
 (16)

One can see that the issue is the same as in the case of previous incidence angle correlation, the design deviation angle can be modelled as $\delta^* = f(\sigma, \theta, \beta_1)$.

2.4.1 Total pressure loss PL

Lieblein in [7] developed an empirical correlation for pressure loss PL as a function of the equivalent diffusion factor D_{eq} [8], based on experimental cascade data for NACA 65-series and C.4 circular-arc blades as

$$PL = \frac{\omega \cos \beta_2}{2\sigma} \left(\frac{W_1}{W_2}\right)^2 = K_1 \left[K_2 + 3.1 \left(D_{eq} - 1\right)^2 + 0.4 \left(D_{eq} - 1\right)^8\right],\tag{17}$$

where $K_1 = 0.004$, $K_2 = 1$ and

$$D_{eq} = \left(\frac{W_{max}}{W_1}\right) \frac{W_1}{W_2} = \left(1.12 + 0.61 \frac{\cos^2 \beta_1}{\sigma} \left(\tan \beta_1 - \tan \beta_2\right)\right) \frac{W_1}{W_2}.$$
 (18)

In presented paper pressure loss is modelled as $PL = f(D_{eq})$. As it can be seen in equations above, the dependency between monitored parameters (α^* , i^* , δ^* , PL), cascade parameters and parameters of the flow is strongly non-linear, that is a suitable task for ANN.

2.5 An approach by employing artificial neural networks

The information processing within neural unit consists of two separated mathematical operations (Gupta, 2013). The first of them is a so-called synaptic operation s which receives inputs and combines them with neural weights that represent some kind of memory. Somatic operation can be responsible for introducing non-linearities as thresholding, non-linear activation, aggregation, etc. This information continues as a nerve impulse into the next layer of neural units is it is shown in Figure 5 (right). Neural output of the individual unit \widetilde{y} is a scalar as it is indicated in Figure 5 (left) and expressed by

$$\widetilde{y} = \sigma(s). \tag{19}$$

N-th order synaptic operation of the neural unit can be written as [9, 10]

$$s = w_0 x_0 + \sum_{i=1}^n w_i x_i + \sum_{i=1}^n \sum_{j=i}^n w_{ij} x_i x_j + \dots + \sum_{i_1=1}^n \dots \sum_{i_N=i_{N-1}}^n w_{i_1 i_2 \dots i_n} x_{i_1} x_{i_2} \dots x_{i_n},$$
(20)

where $x_0 = 1$ stands for threshold and n denotes the length of input feature vector.

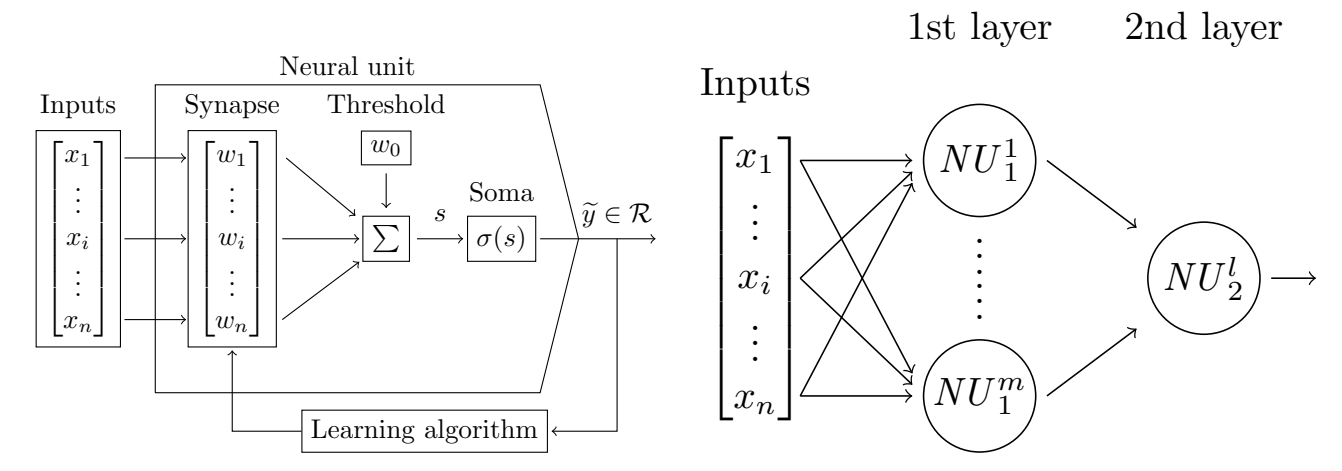


Figure 5 – Neural network: single neural unit (left); shallow neural network (right).

Since desired outputs are known, machine learning is called as supervised learning which is the task of learning a function that maps input to an output. Weight of similarity between neural outputs and true outputs is represented with a cost function \vec{e}

$$\vec{e} = \tilde{\vec{Y}} - \vec{Y}. \tag{21}$$

As we can see, the error is strongly dependent on the neural memories represented by the vector of weights \overrightarrow{W} . Thus, processing of the information should be done in a way which leads to the neural unit being learned. For this purpose, gradient descent batch Levenberg-Marquardt algorithm for weights updating [10] is employed in this work

$$\vec{W} = \vec{W} + \Delta \vec{W},\tag{22}$$

$$\Delta \vec{W}^T = -\left(\vec{\vec{J}}^T \vec{\vec{J}} + \frac{1}{\mu} \vec{\vec{I}}\right)^{-1} \vec{\vec{J}}^T \vec{e}. \tag{23}$$

Coefficient μ is learning rate, \overrightarrow{I} is $n_w \times n_w$ identity matrix, n_w number of weights and \overrightarrow{J} represents $n \times n_w$ Jacobian matrix.

Usually, training data set is divided into three subsets. The first, training set which serves for learning and weights updating. The second is validating set. After each epoch of learning algorithm, error estimation is performed on this subset in order to avoid neural unit overfitting. Training continues until validating error is increasing. Third part is called testing set which measures error after learning is terminated. Testing error after training part was measured as mean squared error (MSE)

$$MSE = \frac{1}{n} \sum_{i=1}^{n} (y_i - \tilde{y}_i)^2.$$
 (24)

2.6 A workflow of the flow field parameters prediction

The procedure begins with calculating α^* because only two parameters are needed as inputs, allowing for an estimation based solely on the geometrical parameters of the cascade, i.e., σ and θ . Next, an estimation of the flow angle β_1 can be made as described in equations (1), and the angles i^* and δ^* can be computed using trained neural networks. Since the flow angles β_1 and β_2 are calculated, the only unknown parameter remaining is the velocity at the cascade outlet, W_2 . The ratio W_2/W_1 can be determined using the following relation [11]

$$W_1 \cos(\beta_1) = W_2 \cos(\beta_2). \tag{25}$$

At this point, all parameters necessary to calculate the equivalent diffusion ratio D_{eq} , as described by equation (18), are known. The final correlation for the design total pressure loss PL can then be applied, as indicated in the prediction workflow shown in Figure 6.

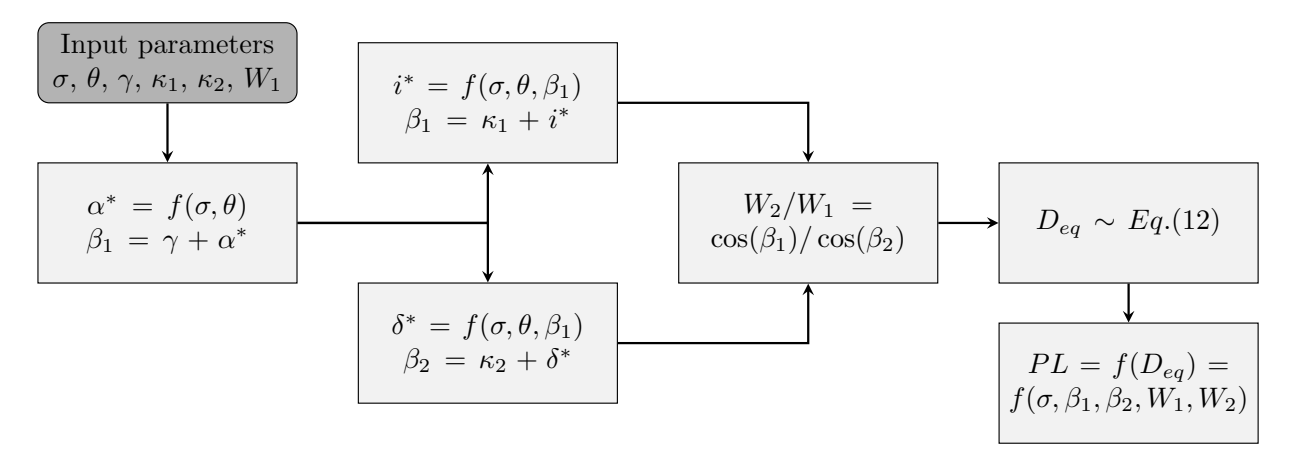


Figure 6 – Workflow for flow parameters prediction.

3. Results

In order to obtain training data set for neural network and replace experimental measurement, various numerical simulations with different geometrical setups and inlet boundary conditions were performed as, *e.g.*, in [12, 13, 14]. Design incidence angle was found through number of simulations as the flow angle with minimum pressure loss as described in [1].

Results of the literature correlations approximation by neural networks, learned on results of CFD simulations as reference data, are presented in the first part of this section, namely design total pressure loss PL, design incidence angle i^* and design deviation angle δ^* .

Second part of the presented results are applications to different abilities of the approximation to speed up flow field investigation. First of them is the prediction of the design incidence angle i^* to find the optimal angle as the input for detailed numerical study of the concrete axial compressor profile, that was excluded from the training data set. The second application is a comparison of the CFD simulation of the whole axial compressor stage against introduced methodology using radial equilibrium with correlations from the literature and approximated correlations using neural networks. Presented results are overall performance parameters and distributions at the rotor outlet - total relative pressure and total pressure loss coefficient Y defined as

$$Y = 1 - \frac{p'_{t,2}}{p'_{t,1}}. (26)$$

Designed neural network is consisted of two neurons in the first layer and single neuron in the output layer as it can be seen in the Figure 5 (right). Synaptic operation of all neurons was assumed as quadratic polynomial in the designed ANN. As the activation function $\sigma(\bullet)$ linear was used in the first layer and in the output layer, respectively.

The data set was divided into three parts - 80% of samples belong to training subset and the rest was equally distributed to validating and testing subsets. Learning rate was set to $\mu = 0.4$ with no decay that allows faster convergence of the neural network learning.

3.1 Approximation of the literature correlations: design total pressure loss PL, design incidence angle i^* and design deviation angle δ^*

In case of design total pressure loss PL, twenty epochs was enough for neural network to learn with testing error 0.0163 as it is shown in Figure 7 (left). Figure 7 (right), shows a comparison of function learned by ANN and Lieblein's correlation against whole data set obtained using CFD.

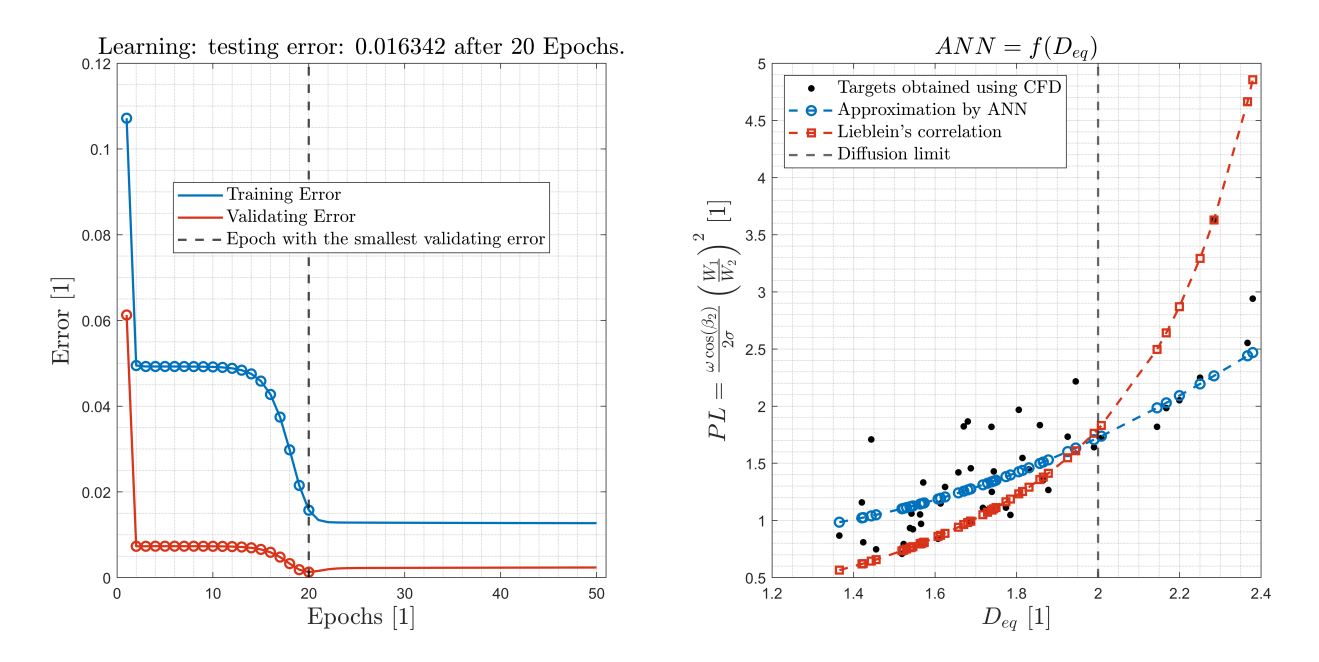


Figure 7 – Progress of the learning (left); ANN results compared to Lieblein's correlation (right).

Correlation for the design incidence angle i^* and design deviation angle δ^* was modelled using the same neural network architecture as for the previous correlation. Prediction of these flow angles using trained neural network and correlations from literature against true targets obtained using CFD can be seen in Figure 8.

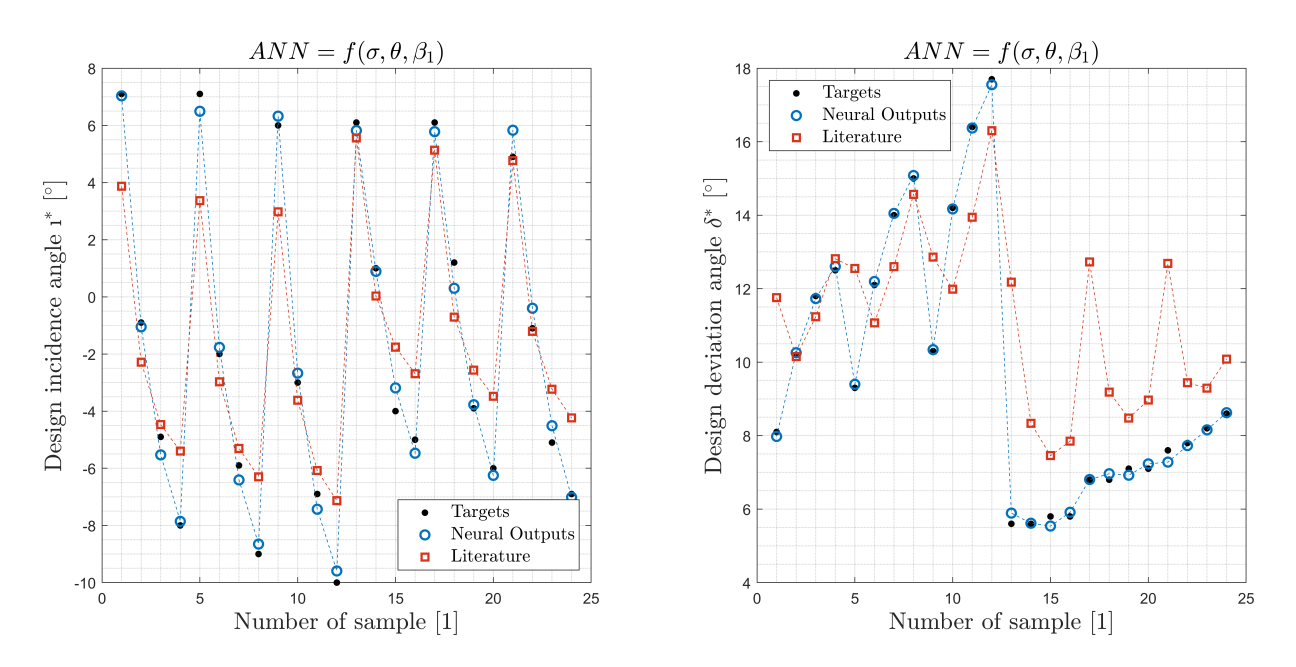


Figure 8 – Predicted flow parameters comparison: design incidence angle i^* (left); design deviation angle δ^* (right).

Table 1 lists deviations measured using MSE defined in equation (24). Results obtained by Lieblein's correlation and by ANN approach are related to data obtained by CFD. As it can be seen, an approximation by ANN is more than three times more accurate than Lieblein's correlation model. In case of flow angles, it can be seen, that the original correlation from literature lack the ability to predict the design flow angles correctly. Comparison with the literature correlations in terms of MSE are also listed in Table 1. It can be seen, that the approach using neural networks is 17 times and more than 250 times more precise in the case of design incidence angle and design deviation angle, respectively.

Table 1 – Results: MSE comparison for the design total pressure loss PL, the design incidence angle i^* and design deviation angle δ^* related to CFD results.

Correlation	Literature	ANN	Literature/ANN	
MSE: PL	0.356	0.109	3.244	
MSE: i*	3.967	0.233	17.026	
$MSE: \delta^*$	4.640	0.018	257.778	

3.2 Optimal incidence angle prediction for airfoil excluded from training data set

As the first outcome of present contribution is a prediction of design incidence angle i^* , that is a thumbling stone, when time consuming 3D CFD simulations have to be performed, because of aforementioned complexity of optimal incidence angle finding and total pressure loss evaluation.

There is a test of neural network predictions performed on the cascade geometry which was not included in the training data set, specifically the cascade with solidity $\sigma = 1.25$, blade angle between the camberline and the axial direction at the leading edge $\kappa_1 = 40^\circ$ and $\theta = 30^\circ$.

The comparison of the design incidence angle estimation and the total pressure loss in the following Figure 9. Angles i_c , i_s denote positive and negative stall incidence angles which bound the range of acceptable incidence angles until total pressure loss increases twice [7, 15].

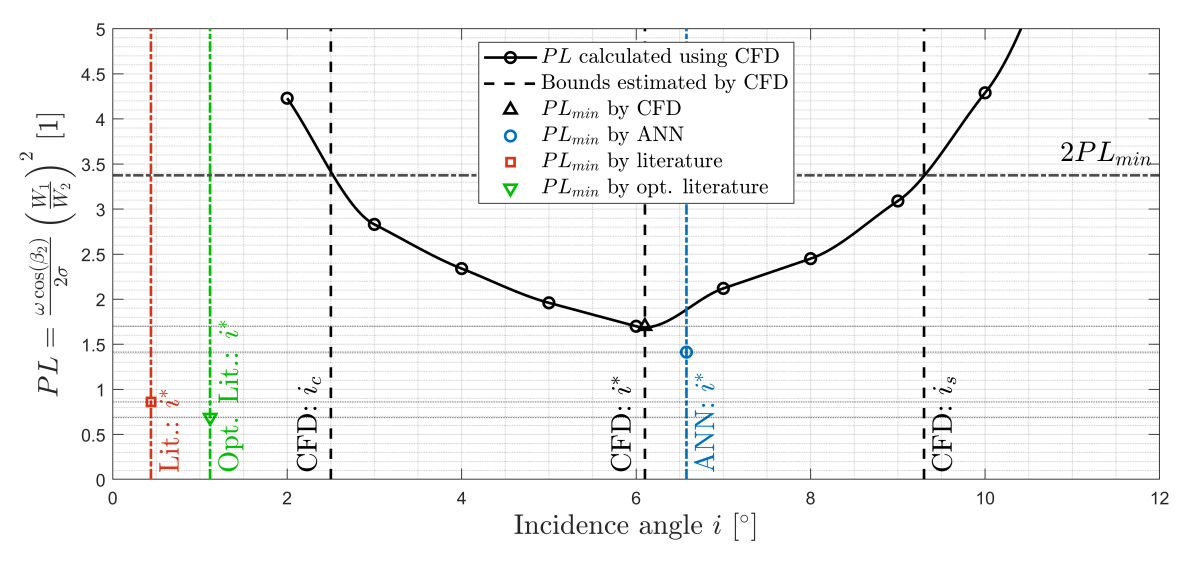


Figure 9 – Results: comparison of incidence angles obtained by literature correlations and ANN.

As it is shown in Figure 9, the design incidence angle predicted by literature correlations is absolutely beyond acceptable incidence angles range. Total pressure loss is also very undershot in case of literature correlation. It seems that design incidence angle should be $i^* = 0.5^{\circ}$. Furthermore, when constants K_{sh} , $K_{t,i}$ in empirical correlations are optimized it resulted into $i^* = 1^{\circ}$, but it results into unsteady simulations in fact and time necessary for the whole process of the compressor design and optimization can be rapidly extended.

3.3 Flow field investigation using radial equilibrium

Further study shows flow field investigation within axial compressor stage containing single rotor and one stator blade row. An illustration of the computational domain is visualized in Figure 10. Mixing plane concept [16] is assumed on the interface between rotating and static parts. Single flow regime was selected for the investigation and following boundary conditions at the inlet was chosen: RPM = 17500, $\dot{m} = 274 \text{kg} \cdot \text{s}^{-1}$, $p_{t,in} = 7.5 \text{MPa}$ and $T_{t,in} = 333.15 \text{K}$.

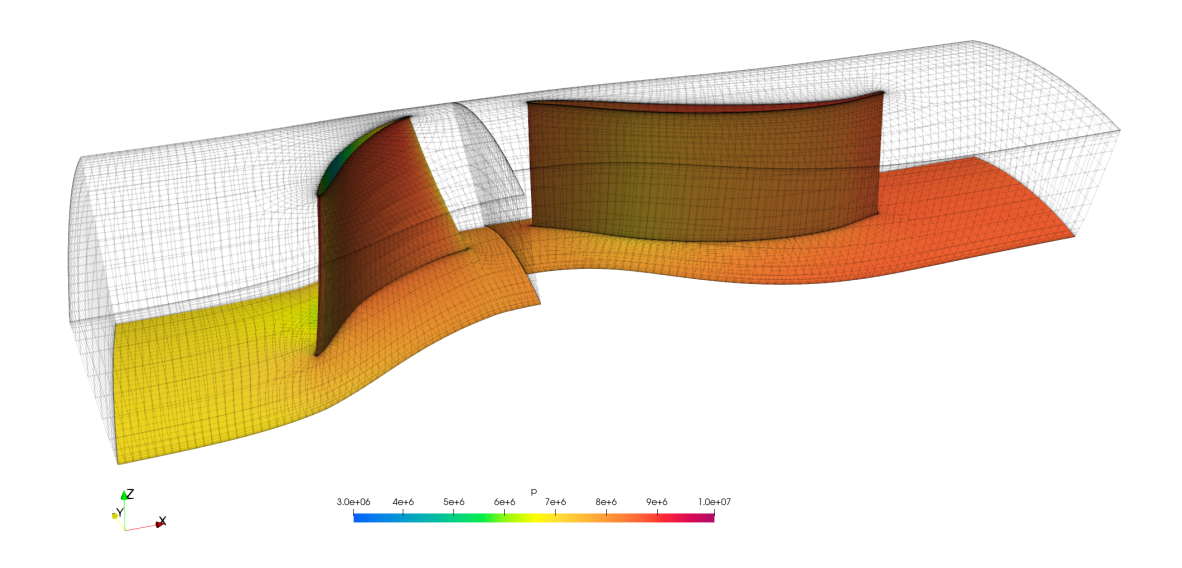


Figure 10 – 3D CFD: Visualization of the computational domain.

In Figure 11, there is a comparison between relative total pressure (and its mean values marked with dashed line), which relates static pressure together with fluid density and relative velocity, obtained through aforementioned approaches. Secondly, there is a comparison of the total pressure loss coefficient distribution *Y* defined by equation (26). It can be seen, that the difference in the approach using neural networks is lower than in case of classical approach using empirical correlations.

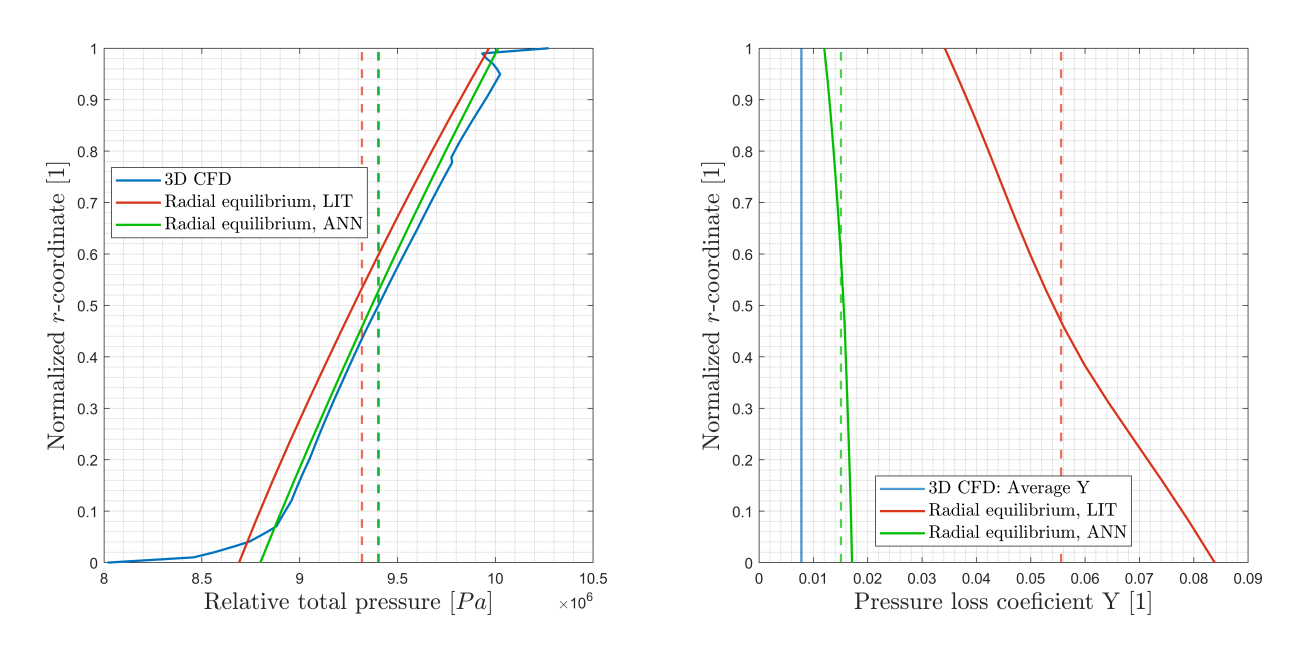


Figure 11 – Comparison of predicted flow field parameters at the rotor outlet: relative total pressure (left); total pressure loss coefficient (right).

In case of CFD results, there is plotted an average of the pressure loss coefficient. It can be seen that pressure drop is captured more precisely using introduced method, that results info different predictions in performance parameters.

Overall pressure ratio PR and efficiency η can be computed based on the total pressure and total temperature at the inlet and at the outlet. Performance parameters are listed in following Table 2. At the first sight, there is not significant difference in pressure ratio PR. On the other hand, when the approach using radial equilibrium equation with empirical correlations from the literature is employed, the prediction is with four percent absolute error in overall efficiency, unlike introduced method using correlations approximated by neural networks, where error decrease to 0.5%.

Table 2 – Results: Performance parameters comparison.

Approach	CFD	Literature	ANN
PR	1.248	1.257	1.221
η	94.9%	91.0%	95.4%

The second and main outcome of present study is, that there can exist an option of surrogate model based on the classical inaccurate empirical correlations can overshot or undershot performance parameters and then possibly optimal geometry can be evaluated as unsuitable.

4. Conclusion & Further work

A machine learning approach in task of fluid mechanics was presented. As the training data set was obtained using comprehensive set of numerical CFD simulations. It turned out, that this approach appears to be a powerful tool for this tasks. Since the neural network is learned, it can perform well in various engineering problems as, *e.g.*, optimal incidence angle determination or flow field parameters prediction within axial compressor.

The main advantage of proposed approach is its fast evaluation of flow field parameters in comparison with precise CFD study. In context of time-expensive CFD simulations it seems that proposed method is a very promising tool in further research and potential method of the axial compressor optimization. Further work should aim to improve the quality of reached results. Since the neural network is learned, it should be able to predict optimal geometrical setup of the compressor cascade for desired design conditions as e.g. inlet velocity or desired deviation angle. Furthermore, optimization process is much more faster because the need for the CFD study can be omitted for early stages of the axial compressor cascade design.

Acknowledgements

Authors acknowledge support from the ESIF, EU Operational Programme Research, Development and Education, and from the Center of Advanced Aerospace Technology (CZ.02.1.01/0.0/ 0.0/16019/ 0000826), Faculty of Mechanical Engineering, Czech Technical University in Prague.

This work was also supported by the grant agency of the Czech Technical University in Prague, grant No. SGS22/148/OHK2/3T/12 and by the Technology Agency of the Czech Republic, project TK03030121 Conceptual Design of an Innovative Safety System for Gas-cooled Nuclear Reactors.

Contact Author Email Address

In case of any question or comment, please do not hesitate to contact the corresponding author on Patrik.Kovar@fs.cvut.cz.

Copyright Statement

The authors confirm that they, and their company or organization, hold copyright on all of the original material included in this paper. The authors also confirm that they have obtained permission, from the copyright holder of any third party material included in this paper, to publish it as part of their paper. The authors confirm that they give permission, or have obtained permission from the copyright holder of this paper, for the publication and distribution of this paper as part of the ICAS proceedings or as individual off-prints from the proceedings.

References

- [1] R. H. Aungier. *Axial-flow compressors: a strategy for aerodynamic design and analysis.* Amer Society of Mechanical, 2003.
- [2] N. P. Salunke and S. A. Channiwala. Design and analysis of a controlled diffusion aerofoil section for an axial compressor stator and effect of incidence angle and mach no. on performance of cda. *International Journal of Fluid Machinery and Systems*, 3(1):20–28, 2010.
- [3] J. Klesa. Aerodynamic design of transsonic compressor airfoil family. *Proceedings of the 36th conference with international participation Computational Mechanics*, pages 115–118, 2021.
- [4] L. J. Herrig, J. C. Emery, and J. R. Erwin. Systematic two-dimensional cascade tests of naca 65-series compressor blades at low speeds. Technical report, NACA, 1957.
- [5] S. Lieblein. Incidence and deviation-angle correlations for compressor cascades. *Journal of basic engineering*, 82(3):575–584, 1960.
- [6] I. A. Johnsen and R. O. Bullock. *Aerodynamic design of axial-flow compressors*, volume 36. Scientific and Technical Information Division, NASA, 1965.
- [7] S. Lieblein. Loss and stall analysis of compressor cascades. *Journal of basic engineering*, 81(3):387–397, 1959.
- [8] S. Lieblein, F. C. Schwenk, and R. L. Broderick. Diffusion factor for estimating losses and limiting blade loadings in axial-flow-compressor blade elements. Technical report, National Advisory Committee For Aeronautics Cleveland OH Lewis Flight, 1953.
- [9] M. Gupta, L. Jin, and N. Homma. *Static and dynamic neural networks: from fundamentals to advanced theory*. John Wiley & Sons, 2004.
- [10] M. Gupta, I. Bukovsky, N. Homma, A. Solo, and Z. Hou. Fundamentals of higher order neural networks for modeling and simulation. In *Artificial Higher Order Neural Networks for Modeling and Simulation*, pages 103–133. IGI Global, 2013.
- [11] S. Farokhi. Aircraft propulsion. John Wiley & Sons, 2014.
- [12] O. Bublík, V. Heidler, A. Pecka, and J. Vimmr. Neural-network-based fluid-structure interaction applied to vortex-induced vibration. *Journal of Computational and Applied Mathematics*, page 115170, 2023.
- [13] P. Kovář and J. Fürst. Compressor cascade total pressure loss correlation modelling at design points using artificial neural networks. *Proceedings of the 37th conference with international participation Computational Mechanics*, pages 50–53, 2022.
- [14] P. Kovář and J. Fürst. Compressor cascade correlations modelling at design points using artificial neural networks. 2023.
- [15] A. R. Howell. Fluid dynamics of axial compressors. *Proceedings of the Institution of Mechanical Engineers*, 153(1):441–452, 1945.
- [16] INC Fluent et al. Fluent 6.3 user's guide. Fluent documentation, 2006.